RSC Advances

ROYAL SOCIETY OF CHEMISTRY

www.rsc.org/advances

Journal Name

RSCPublishing

ARTICLE

Precise pooling and dispensing of microfluidic droplets towards micro- to macro-world interfacing

Cite this: DOI: 10.1039/x0xx00000x

Eric Brouzes[a,*], April Carniol[a], Tomasz Bakowski[a] and Helmut H. Strey[a]

Received 00th January 2012,
Accepted 00th January 2012

DOI: 10.1039/x0xx00000x

www.rsc.org/

Droplet microfluidics possesses unique properties such as the ability to carry out multiple independent reactions without dispersion of samples in microchannels. We seek to extend the use of droplet microfluidics to a new range of applications by enabling its integration into workflows based on traditional technologies, such as microtiter plates. Our strategy consists in developing a novel method to manipulate, pool and deliver a precise number of microfluidic droplets. To this aim, we present a basic module that combines droplet trapping with an on-chip valve. We quantitatively analyzed the trapping efficiency of the basic module in order to optimize its design. We also demonstrate the integration of the basic module into a multiplex device that can deliver 8 droplets at every cycle. This device will have a great impact in low throughput droplet applications that necessitate interfacing with macroscale technologies. The micro- to macro- interface is particularly critical in microfluidic applications that aim at sample preparation and has not been rigorously addressed in this context.

Introduction

We present the design of a microfluidic device that accurately and automatically pools and delivers a precise number of droplets. It will permit the interfacing of the microfluidic world to the macrofluidic world (e.g. microtiter plates) and will allow the seamless integration of droplet microfluidics into already developed robotic workflows. The approach combines passive droplet trapping[1, 2] and on-chip valves[3-5], two robust microfluidic technologies which have rarely been combined together[6-8]. The novel aspect of our design is that the valves are an integral part of the traps themselves.

The benefits of microfluidic techniques stem from the low reaction volumes used that allow for better control of reaction conditions such as flow patterns or reactant concentrations. In contrast to analytical assays where detection can be performed on-chip, some methods that benefit from microfluidic format necessitate the transfer of products to macroscale technologies for the analysis of samples. This is particularly true for single-cell analysis techniques that clearly benefit from reduced reaction volumes and microfluidic handling techniques. For instance, the droplet format is ideal for manipulating or processing single-cells since it allows multiplexed sample processing in isolated and independent reactors that can be displaced and retrieved without any loss of material[9-14]. In addition, an automated micro- to macro- interface for droplet microfluidics would be attractive for simply depositing single-cells encapsulated in droplets[15, 16] into microplates for further analysis by ELISA, or processing for single-cell genomics, proteomics or metabolomics. Such an automated system would replace the use of expensive and high-maintenance FACS machines currently used to perform such tasks.

In the case of single-cell genomics, nucleic acids extraction amplification and possibly barcoding can be prepared in droplets. The low volume of droplets has a decisive advantage to perform high-quality amplification of the minute amount of DNA present in single-cells, because it allows maintaining single-cell genomic DNA at concentrations that are in the range of efficient molecular reactions. However, the synthesis of the sequencing library necessary to analyse the genomic content of the sample would require transferring the amplified material into microtiter plates. These methods become highly significant as single-cell genomics technologies mature into a viable clinical tool for cancer diagnostics[17, 18].

From these examples, it is clear that there exists a need for a robust method to allow precise control and routing of droplets and their interfacing with a microtiter plate format in order to fully exploit the advantages of droplets in sample preparation applications such as single-cell genomics. Currently, except for electrowetting techniques[19-21] that require intricate microfabrication and control, there is no method to manipulate a precise and intermediate number of droplets. The droplet manipulation presented herein is based on robust principles and can be easily automated. Our approach permits to optimize the efficiencies of molecular reactions by keeping reactant concentrations in their optimal ranges by using either small volume or bulk formats where most appropriate. The micro- to macro- interface is particularly critical in microfluidic

applications that aim at sample preparation and has not been rigorously addressed in this context before.

Material and methods

Microfluidic chip fabrication

Chips are PDMS/glass hybrids fabricated using soft-lithography and off-stoichiometry as already described[8, 27]. In brief, we designed microfluidic circuits with the DraftSight software (Dassault Systems, Paris) and had them printed at 25,400 dpi resolution onto a Fuji transparency mask (CAD/Art Services Inc., Bandon, Or). Using the mask, we fabricated a master using a negative photoresist SU8-2025 (Microchem, MA) that is evenly spun onto a 3 inch silicon wafer and patterned by photo-litography (Newport 500W UV-illumination system). This procedure creates rectangular channels.

Masters to make rounded channels are generally fabricated using a positive photoresist that generates rectangular channels that can be rounded by a heat treatment[8, 28]. Raising the temperature above the glass transition temperature of the photoresist allows it to relax into a rounded shape that minimizes surface energy. Here, we developed an alternative method to create the rounded channels that we use to prevent valve leakage (Fig. 4c). We spin-coated a solution of negative photoresist SU8-2007 to create a 7 µm layer on top of the already developed rectangular channels. The shallow and low viscosity layer relaxes to minimize surface energy and creates a rounded dome on top of otherwise square 35 µm deep channels. We then used a mask to limit the rounding of channels to specific locations. Valves were in "push-up" configuration with the microfluidic layer on top of the valve control layer.

We used PDMS (Sylgard 184, Corning) at 1:5 weight ratio of curing agent: polymer base for molding the microfluidic layer, and at 1:17 weight ratio for the valve control layer. After mixing, the 1:17 PDMS solution was degassed for 10 minutes, and the 1:5 PDMS solution poured on the microfluidic master before degassing for 25 minutes. After 10 minutes, the 1:17 PDMS solution was poured on the valve control master and further degassed for 15 minutes. The 1:17 PDMS solution was then spin-coated at 1,500 rpm for 50 seconds. Both masters were cured in an 80°C oven for about 9 minutes and 12 minutes for the microfluidic layer and the valve control layer respectively.

We noticed a great variation in the curing time required based on the lot of the PDMS components. Our rule of thumb is to cure each layer until they just lose their "stickiness" upon a gentle touch with a glove. Once cured, the microfluidic layer was unmolded, mounted on a glass slide with channels up by capillarity and aligned on top of the control layer using a mask-aligner (Newport 500W UV-illumination system) equipped with an inspection monocular microscope, camera and coaxial illumination (Amscope). Once aligned, the microfluidic layer and the valve control master were clamped between a glass slide and an aluminum plate with two binder clips. This sandwich was then degassed for 10 minutes before being cured at 80°C for 2 hours. After curing, we punched the access holes into the PDMS (Syneo, US), and bonded it to a glass slide by oxygen plasma activation (PDC-32G, Harrick plasma). The assembled chip was sandwiched between aluminum plates held by binder clips. After a 80°C overnight baking, channels were treated with a fluorinated tri-chloro silane reagent[29] (heptadecafluoro-1,1,2,2-tetrahydrodecyl)trichlorosilane, Gelest, PA) diluted at 1% wt in FC3280 oil (3M). The solution was injected into channels with a disposable syringe, through a hydrophobic 0.2 µm disc filter and a blunt needle, and flushed out with FC 3283 oil after a few minutes of incubation.

We created the electrodes using dedicated channels that we injected with low-melting solder (Cerrolow-117, 47°C melting temperature). The connections are assured by inserting electric wires into the channel inlets reinforced with a short piece of 1/16" OD x 0.04" ID peek tubing (Idex).

Scanning Electron Microscope images of photoresist masters (Fig. 4c) were taken using a Hitachi S-4800 SEM (JEOL, USA, Inc., Peabody Massachusetts). Images were acquired using a 5 kV accelerating voltage, 10 µA beam current, 40-57 mm working distance, and a stage tilt angle of 45-57 degrees. Because of the relatively large size of the structures under observation, only the low magnification setting was used (< 350X).

Designs with dimensions

All channels were 35 µm deep as measured with a stylus profilometer (Dektak 150) using a 2 µm radius tip. In all designs, the bypass channel was 2,050 µm long and 70 µm wide. The rectangle trap was 135 µm long and 110 µm wide and its leak channel is 110 µm long and 20 µm wide; the Laplace channel was 195 µm long, its wide base was 110 µm, its narrow base was 25 µm and its leak channel was 97.5 µm long and 20 µm wide. Microfluidic anchors that sit on top of each trap had a diameter of 50 µm and were 35 µm deep. To design the pooling-fusing delivery droplet module, we added a 1,095 µm long and 90 µm wide chamber that was lined up with 5x 60 µm long and 25 µm wide side channels with an additional 6th side channel closest to the chamber that was 85 µm long and 30 µm wide.

We designed the multiplex system as a series of pairs of trapping-delivery modules because it was practically impossible to design delivery channels such that the flow was equal in all branches when delivery valves were open (Supp. Fig. 4 for an equivalent electric circuit). Using equations 1 and 2 below to estimate the hydrodynamic resistance of channels[30], we designed delivery channels as 1,200 µm long, 80 µm wide for the first delivery channel and 147 µm wide for the second channel. Adding small corrections to account for the complete design we estimate a 53:47 flow split between the two delivery channels when the valve was open.

$$P = c\eta \frac{l}{wh^3} Q \quad (1)$$

with

$$c = 12\left[1 - \frac{192}{\pi^5}\frac{h}{w}\,tanh\left(\frac{\pi w}{2h}\right)\right]^{-1} \quad (2)$$

where Q is the flow rate and l, w and h represent the length, width and height of the channel and η is the fluid viscosity. We used these equations as a guideline here, being aware that the use of rectangular channels and of a bi-phasic system limits their accuracy.

Microfluidic set-up

The microfluidic station is based on an inverted microscope (Motic, AE31) equipped with a custom stage. The microscope is equipped with a Firewire camera (Scout scA640-120fm, Basler), and the illumination is provided by a high power LED (Luxeon) driven by a MOSFET circuit connected to one of the digital output pins of a multifunction data acquisition card (NI PCIe-7841R, National Instruments). Using this setup, we can control the camera and synchronize the image acquisition and illumination using an application developed under Labview environment (National Instruments). The system permits stroboscopic exposure in which an image can be captured over the period of 2 illumination pulses. This feature allows the experimental measurement of droplet velocity.

Fluids are actuated by a set of pressure controllers with a 0-15 psi pressure range (MPV1, Proportion Air) mounted in parallel onto a manifold. They are controlled by a Labview (National Instruments, TX) application via a microprocessor-based (Arduino) interface by serial communication. Fluids are loaded into 1mL or 15mL tubes equipped with custom designed teflon caps that serve as ports to connect 1/32" peek tubing (Idex). 1/32" peek tubing is directly inserted in chip inlets and outlets.

We injected valves with FC40 oil which was surmounted in the reservoir by mineral oil to isolate fluorinated oil from pressurized air. Valves were actuated by a manifold valve controller (Model EMC-08, Clippard), controlled by a custom software developed under Labview via an Arduino microprocessor. We used a nominal pressure of 35 psi to actuate on-chip valves.

We used PBS and 1% PEG-based fluorinated surfactant[31] dissolved in HFE 7500 oil to generate emulsions of 0.6 nL droplets employing a flow-focusing nozzle[1]. Droplets were collected into a vessel made of a 3 inch long and 15 mm diameter Trubore glass tubing (Ace glass Inc, NJ) capped by 2 custom designed teflon inserts that serve as ports to connect 1/32" peek tubing (Idex). The glass tubing was treated with the same fluorinated tri-chlorosilane solution used for channels to ensure good emulsion stability. We used a solution of 1% PEG-based fluorinated surfactant dissolved in FC40 to space droplets during re-injection into the delivery chip. We used HFE7500 fluorinated oil to generate, collect and store droplets that have lower interfacial tension which assures higher droplet stability; and we used FC40 fluorinated oil to space droplets during reinjection to increase their interfacial tension for improved trapping.

Interfacial tensions were measured using the pendant drop method. Dark droplets contain Bromophenol blue at 0.05% weight in PBS. Colored channels in the central panel of Figure 5 were obtained by injecting a solution of food icing color (Wilton Industries, IL) diluted 1:4 with water.

All videos, except Supp. Movie 4, were generated from stacks of images taken with the microfluidic set-up at 10x magnification and saved as avi-files using Fiji software, and further compressed using Avidemux (http://avidemux.sourceforge.net/). Supp. Movie 4 was taken under a stereomicroscope (Stemi SV6, Zeiss) mounted with a Casio EX-F1 onto one of the oculars via an adapter (Zarf Enterprises). Supp. Movie 6 has been edited using Movie Maker (Microsoft).

Image processing

Images used in figures have been minimally manipulated using Fiji (http://fiji.sc/Fiji) and Photoshop (Adobe) softwares. To correct for uneven illumination, we corrected the background using the "Subtract Background" function in Fiji. We adjusted the contrast and sharpness of images using the "curves", the "exposure", and the "smart sharpen" functions in Photoshop. In rare cases we used the "Clone Stamp Tool" from Photoshop to erase a contaminant that did not interfere with the functioning of the chip but would have been distracting in the figure. This is the case in Fig. 5b where a fiber was trapped between the PDMS slab and the glass slide. The videos have been edited only for length and image size, and the aforementioned fiber can be seen in supplemental video Supp. Movie 3.

Optimization of trapping efficiency

Droplets (0.6 nL) were generated on chip by encapsulating PBS into 1% PEG-based fluorinated surfactant dissolved in FC40 oil. Droplets were stored in an on-chip reservoir and further pushed into the traps. After one droplet was trapped, we injected droplets at different pressures and recorded a series of images using the stroboscopic system to measure droplet velocity. For our analysis, we selected cases for which no droplets are present in the bypass system in order to ensure consistent resistance of the bypass. We used droplet velocity because pressure values were dependent on the overall number of droplets present in the reservoir. For all velocity measurements, we measured droplet velocity at the same location before the trap (described in Supp. Fig. 3). We used the Fiji software to measure the distance travelled by droplets between two illumination flashes by employing ruler marks on the chips for calibration.

Results and discussion

To interface droplet microfluidics with macro-scale technologies, our strategy consists in developing a microfluidic device that accurately pools and delivers a precise number of droplets. The device relies on a basic module that first traps and then delivers droplets. Each cycle consists of a trapping, clearing and delivery phases. We proceeded to derive another module that allows droplet pooling before delivery. We then sought to improve the basic module by: 1) optimizing its

trapping efficiency; 2) uncoupling the droplet loading and delivery phases. Finally, we integrated the basic module into a device that can perform multiplex droplet delivery.

Basic module for droplet trapping and dispensing

The basic module used to trap and dispense droplets combines a droplet trapping chamber[22], and an on-chip push-up valve[8] that serves as one of the walls of the trapping chamber (Fig. 1a). We first load a droplet into the trap and then deliver it into the dispensing channel by opening the valve. The droplet trap consists of a bypass channel that winds around a unit made of the trapping chamber connected to a small leak channel[22] (Fig. 1a). The hydrodynamic resistance of the bypass channel is higher than the resistance of the leak channel, such that the first droplet to flow into the unit enters the chamber. As a result, this droplet obstructs the leak channel and blocks any further flow down the chamber (Fig. 1b). The following droplets follow the streamlines and flow through the bypass channel (Fig. 1c). The parking of droplet is passive and relies on the change of hydrodynamic resistance due to the trapping of droplets.

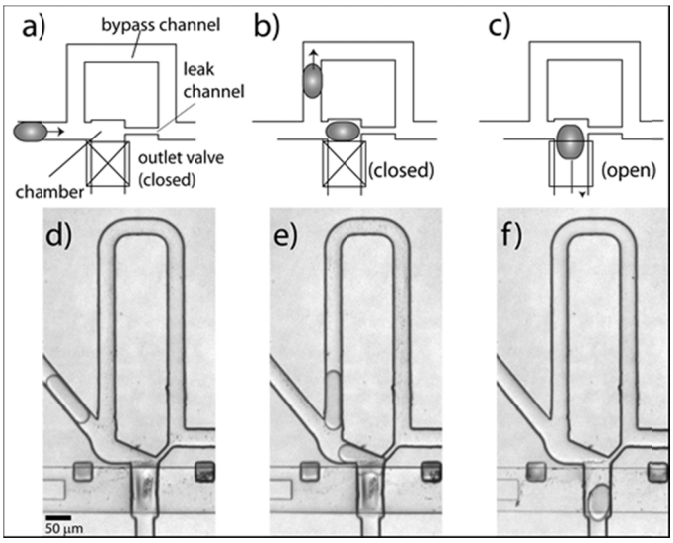

Fig. 1 Strategy to dispense single droplets. The design combines a droplet trap and an on-chip valve. a,d) An incoming droplet (0.6 nL) follows the path of least hydrodynamic resistance and enters the trapping chamber. b,e) The presence of a trapped droplet blocks further flow into the chamber and forces following droplets to flow down the bypass channel. c,f) Once the bypass channel is cleared from other droplets, the trapped droplet is released by opening the on-chip valve.

Figure 1 depicts the sequence of events for delivering a single droplet into the dispensing channel: 1) we re-inject an emulsion to load a droplet into the trapping chamber (Fig. 1d); 2) we clear the excess of droplets present in the bypass channel by reducing the emulsion pressure and increasing the oil pressure (Fig. 1e); 3) we release the trapped droplet by opening the on-chip valve and increasing the oil pressure (Fig. 1f). We can repeat the sequence of events for several cycles in a semi-automated fashion (Supp. Movie 1).

To accommodate larger droplets we increased the volume of the trapping chamber and added a leak channel that connects the chamber to the bypass channel (Supp. Fig. 1). This design allows for better trapping of droplets and avoids splitting of larger droplets at the bifurcation. Alternatively, this modification permits the trapping of several smaller droplets (Supp. Fig. 1, 1x 1.44 nL droplet or 2x 0.8 nL droplets).

Pooling-delivery module

In multiplexing applications it may be advantageous to pool a precise number of droplets before delivery. In single-cell genomics, for example, each droplet would contain genomic material from a single-cell. This material would have been uniquely barcoded in order to identify the contribution of each single-cell to a multiplex sequencing reaction.

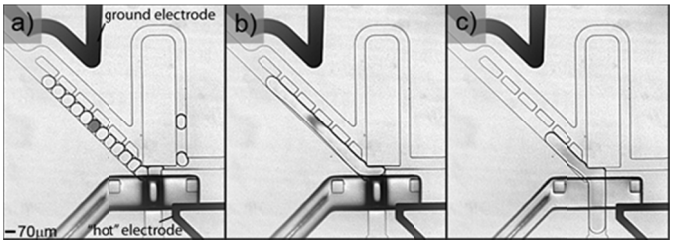

Fig. 2 Strategy to pool and dispense a precise number of droplets. In this case, the trapping chamber is extended to a volume of 3.9 nL and a series of side leak channels is inserted. A couple of electrodes spans across the trapping chamber. a) Droplets are first trapped in the chamber. b) After clearing of the bypass channels, an electric field triggers the fusion of the trapped droplets. c) Finally, the on-valve chip is opened to dispense the pooled droplet through the dispensing channel.

To achieve such droplet pooling we expanded the previous design developed for large droplets by using an even larger trapping chamber and a whole series of side leak channels that connect the chamber to the bypass channel (Fig. 2; Supp. Movie 2). We electro-fuse the pooled droplets into a single large droplet, using a pair of electrodes that span the trapping chamber, to avoid droplet dispersion along the channels and keep them in a single packet for efficient delivery. We trap droplets, clear the bypass channel (Fig. 2a), and then apply a high-voltage high-frequency electric field[27] through the electrodes for 1 second (Fig. 2b) before dispensing the pooled content into the delivery channel (Fig. 2c). The precise number of droplets that can be pooled is purely determined by the volume ratio of the trapping chamber and the droplets: the trapping chamber fills until the furthest side leak channel is blocked which allows pooling a different number of droplets as a function of their volume (Supp. Fig. 2). These results demonstrate the ability of our microfluidic chip design to pool and dispense any precise number of droplets, and highlight the use of side leak channels to allow trapping of droplets with different volumes employing the same basic design principles.

Optimization of trapping efficiency

The durations of the loading and clearing phases depend on the pressures used to flow droplets into and through the system: the higher the pressures, the faster the droplets and the shorter the durations of these phases. However, trapped droplets will deform and flow through the leak channel if the pressures are too high. Droplets can actually escape the trapping chamber

following two scenarios: when either the loading or clearing pressures are too high, or when another droplet flows through the bypass channel with a sufficiently high velocity. We sought to optimize the efficiency of droplet trapping in order to use higher pressures and speed up the loading and clearing phases. To do so, we measured the efficiency of different designs where the trapping chamber consists either of a rectangular chamber (Fig. 3a) or a Laplace trap[26] (slotted trap) (Fig. 3c). We also derived a new version of each design by adding a microfluidic anchor[32] (Fig. 3 b,d). We quantified the trapping efficiency of each design by measuring the lowest or critical velocity at which a droplet flowing through the bypass channel helps dislodge the trapped droplet (Fig. 3 and Supp. Fig. 3). This approach permits to disregard the state of the rest of the circuit (e.g. how many droplets are present in the reservoir).

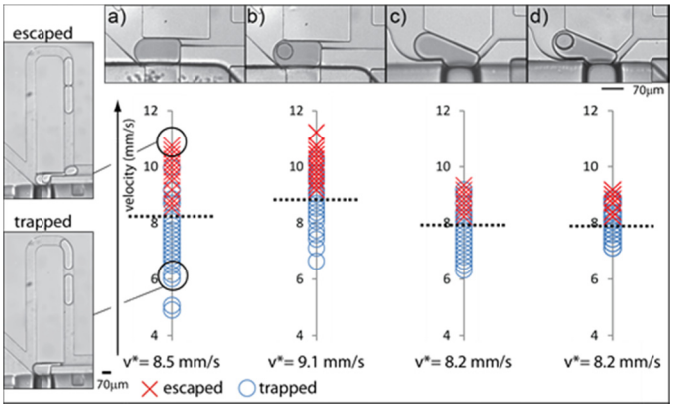

Fig. 3 Optimization of trapping efficiency. We compared the trapping efficiency of four designs (upper panel): a) rectangle trap; b) rectangle trap with a microfluidic anchor; c) a Laplace trap; and d) a Laplace trap with a microfluidic anchor. To measure the trapping efficiency of the designs, we trapped a droplet and we monitored the effect of a second droplet on the trapping stability as a function of its velocity (left vertical panels). We used the lowest destabilizing velocity or 'critical" velocity at which the trapped droplet is released to compare the trapping efficiency of the designs (lower right panel). The rectangle trap with the microfluidic anchor exhibited the most stable or efficient trapping.

From this experiment and the theoretical derivation of the trapping energy of the different designs we could infer four principles.

First, the critical velocities range from 8.2 mm/s to 9.1 mm/s and thus are not strongly affected by the design variations tested here (Fig. 3). This indicates that droplet trapping is dominated by the effect of the leak channel. We could thus increase the trapping efficiency by simply increasing the length of the leak channel, but this solution is complicated by the requirement that its hydrodynamic resistance remains lower than the hydrodynamic resistance of the bypass channel. Droplets may also break up when flowing through a long and narrow channel. For these reasons we tested other strategies to improve the trapping efficiency without elongating the leak channel.

Second, our experimental analysis shows that the microfluidic anchor provides an improvement to droplet trapping (Fig. 3). A microfluidic anchor allows a confined droplet to relax into a cavity and thus lower its overall interfacial energy by reducing its interface area [33]. Assuming that the relaxed surface adopts the shape of a half-sphere of diameter equal to the diameter d of the anchor and that the droplet has a constant volume, we can estimate the upper limit of the trapping energy of a microfluidic anchor in our configuration by the following formulation (see supplemental data):

$$\mathrm{E}_{microfluidic\ anchor} \leq \gamma\,\pi d^2\left(\frac{1}{2}-\frac{w+h}{6wh}\,d\right)$$

where γ is the interfacial tension, d, w and h are respectively the =diameter of the anchor, the width and the height of the trapping chamber. If we use the same energy argument and assume in first approximation that the trapping energy of the leak channel is equivalent to the energy necessary to create an interface to fill the leak channel while maintaining the droplet volume constant, the trapping energy of the leak channel can be written as (see supplemental data):

$$\mathrm{E}_{leak\ channel} = 2\gamma h l_{leak}\left(1-\frac{w_{leak}}{w}\right)$$

where γ is the interfacial tension, h, w, l_{leak} and w_{leak} are the height and the width of the trapping chamber, and length and the width of the leak channel respectively. Computing these energies for our configuration shows that the trapping energy due to the leak channel is 5-fold higher than the trapping energy due to the microfluidic anchor. This theoretical evaluation is in qualitative agreement with our experimental data that show a real but limited increase in the critical velocity for the rectangular trap augmented with the microfluidic anchor compared to the simple rectangular trap (Fig. 3).

Third, the critical velocities for the designs with the Laplace trap are lower than the rectangular configurations. The Laplace trap relies on geometrically inducing a differential in curvatures between the front and the back of the droplet by using a slotted trap. This differential in curvatures corresponds to a differential in Laplace pressure that keeps the droplet trapped[26]. The advantage of the Laplace trap is that it accommodates droplets of different sizes, but by doing so it compromises the trapping efficiency. When a droplet enters and passes through the leak channel, the curvature at its back is fairly constant in the case of the rectangular trapping chamber while this back curvature increases in the case of the Laplace trap. As a consequence the difference in Laplace pressure between the front and the back of the droplet remains mostly constant in the case of the rectangular trap but decreases while the droplet is leaving the chamber in the case of the Laplace trap. In this latter situation, the trapping force progressively decreases as the droplet enters and passes through the leak channel. This explains why the Laplace trap has a negative effect on the trapping efficiency of the leak channel compared to the rectangular trap (Fig. 3).

Fourth, independent of the design trapping, energy is proportional to the interfacial tension and the higher the interfacial tension the more efficient the trapping. This has practical implications because the interfacial tension of the system can be modulated by using different types of fluorinated

oil. For instance, the water-oil interfacial tension for the PEG-based Krytox surfactant at 2% wt. in FC 40 has been reported at 20 mN/m[33], while we measured the water-oil interfacial tension of the same amount of surfactant in HFE7500 at 1 mN/m. For this reason, we adopted the strategy of using HFE7500 oil with 1% surfactant to generate, collect and store droplets; and of using FC40 oil with 1% surfactant to re-inject, clear and deliver droplets. In this manner, we take advantage of the interfacial properties of both formulations to assure excellent droplet stability and efficient trapping.

Strategy to uncouple droplet loading and delivery using air

We further improved the cycling time for the droplet delivery by uncoupling the trapping-clearing and the delivery phases. In the initial configuration shown in Fig. 1, the system cannot start the next loading phase until trapped droplets are delivered to the final vessels. To circumvent this limitation, we added an additional control channel connected to delivery channels downstream of the delivery valves (Fig. 4a).

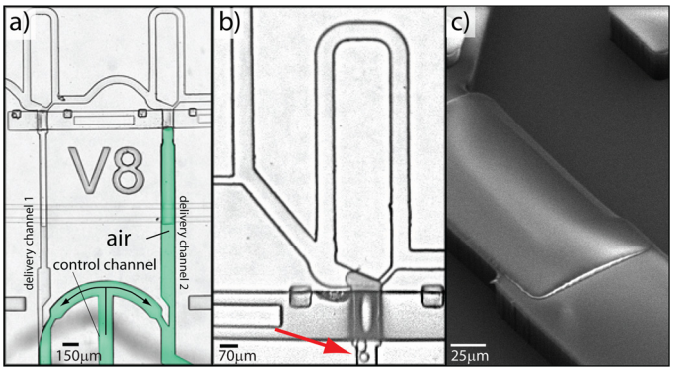

Fig. 4 Strategy to uncouple droplet loading-clearing and delivery phases. In order to optimize the cycling time of the device we uncoupled droplet loading-clearing and delivery by adding channels downstream of the delivery valves to control final droplet delivery. In addition, we deliver droplets with air to minimize the use of oil and its presence in the target vessel. a) We added a control channel to a 2-plex delivery system to transfer droplets into the bottom delivery channels with air (in green). Arrows indicate air flow. b) Valves made with rectangular channels are "leaky" and create problems such as extrusion of droplets (red arrow) or poor isolation of the trapping side from the air delivery module. c) We developed a novel microfabrication method to "round-up" channels using the negative photo-resist SU8 and create tight valves necessary to use air delivery.

These additional control channels can be inter-digitized with the different trapping lines such that only a single channel is capable of actuating delivery. We also opted to deliver droplets using air rather than oil for two reasons: 1) we aim to minimize surfactant consumption and to reduce the amount of oil in the final vessel in order to lower the risk of interference on subsequent molecular reactions; 2) the viscosity of air is lower than the viscosity of the fluorinated oil and therefore allows a faster delivery.

Practically, our strategy necessitates tight fitting valves in order to avoid injection of air into the droplet trapping modules, and to avoid droplet extrusion through improperly sealing valves (Fig. 4b). Push-up valves made with rounded channels provide the best seal; and we developed a novel method to fabricate this type of valve using a negative photoresist in order to simplify chip microfabrication (Fig. 4c and Methods for details).

Multiplex delivery of droplets

The robustness of the basic module permits its multiplexing into a single device and thus to optimize the cycling time of droplet dispensing. Our objective was to simultaneously transfer multiple trapped droplets into delivery channels in a minimum amount of time such that valves could be rapidly closed to start the next loading phase. We initially pursued the simultaneous delivery of all droplets, which required the balancing of the hydrodynamic resistance of the different branches in order to even the oil flow through all the delivery channels. However, the electrical analogy to hydrodynamic circuits shows that it is practically unfeasible to design delivery channels that accommodate such a constraint (Supp. Fig. 4). We therefore chose to assemble the 8-plex delivery device as a series of four pairs of trapping-delivery modules where both branches are equilibrated (Fig. 5 central panel). As a consequence of this design choice, the device uses four independent valves for trapping-delivery. When all valves are open, most of the oil is diverted through the first module because of the accrued resistance of the subsequent branches of the trapping modules. Hence proper multiplex droplet delivery is obtained by a sequence where all the delivery valves are first open and then sequentially closed starting with the valve closest to the re-injection nozzle.

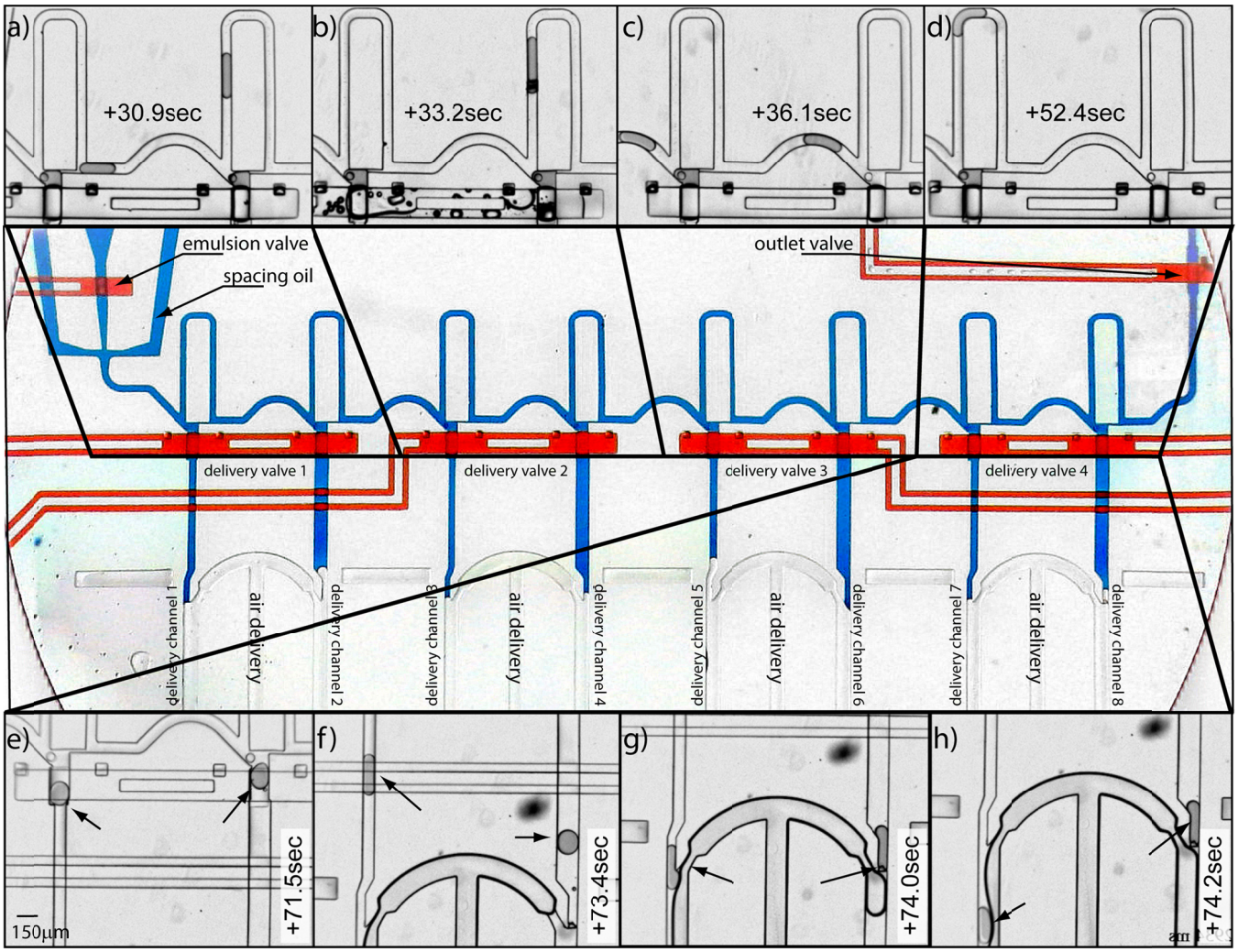

Fig. 5 Multiplex delivery system. We developed a system that permits the multiplexed delivery of 8 droplets. Central panel: It comprises a nozzle to re-inject an emulsion into the system (left). For hydrodynamic reasons, the device is based on a series of four pairs of trapping modules that are controlled by independent valves (red structures). The sequence of events is the following: a-d) injected droplets flow down to the next available traps until those are all filled and the excess of droplets is flushed out of the system. The emulsion retracts in the inlet by balancing pressures and the valves controlling the inlet and the outlet are closed. e-h) the air pressure is then lowered, the delivery valves are opened and the oil pressure is increased to transfer droplets into the delivery channels (arrows). The delivery valves are then sequentially closed from the left to the right. This is necessary because the hydrodynamic resistance increases from left to right which leads to an uneven delivery across the traps where most of the flow goes through the first pair of open droplet traps. By closing the valves sequentially we achieve a rapid, sequential and consistent delivery. Once all droplets moved into their respective delivery channels, delivery valves are closed, the air pressure is raised, and the cycle can start again. a) shows the first pair of traps; b) the second pair; c) the third; and d-h) the fourth pair of traps.

The whole delivery cycle for the multiplex delivery of droplets includes the following steps (Supp. Movies 3 and 4): 1) we re-inject droplets by adjusting the pressures of the emulsion and the spacing oil to allow proper droplet injection while we maintain the emulsion and the outlet valves open. Droplets flow down to the next available traps until those are all filled; 2) we flush the excess of droplets out of the system by increasing the pressure of the spacing oil (Fig. 5a-d). The emulsion retracts into the inlet after lowering the emulsion pressure; 3) we close the emulsion and outlet valves; 4) we lower the air pressure, open the delivery valves and we increase the pressure of the spacing oil to transfer droplets into their respective delivery channels; 5) we sequentially shut the delivery valves to avoid diverting most of the oil in the first two delivery channels; 6) we finally raise the air pressure to complete the cycle and assure final droplet delivery (Fig. 5e-h).

Our multiplexing scheme possesses an auto-correction feature that permits to correct situations where a droplet skips a trapping chamber (Fig. 6 and Supp. Movie 5). When a droplet does not enter an empty chamber but rather flows through the bypass channel, its velocity greatly decreases because most of the oil flows through the un-obstructed leak channel. Meanwhile, the following droplet has a higher relative velocity and reaches the module before the skipping droplet has flowed through the entire bypass channel. The presence of the first droplet increases the apparent resistance of the bypass channel which prompts the second droplet to enter the trapping chamber. The intrinsic correction feature is such that a skipping droplet will assure that the following droplet enters the skipped chamber. This correction mode suggests injecting a number of droplets slightly higher than the multiplexing capacity of the

device. Surplus droplets can then be collected into an on-chip or off-chip reservoir and be later re-injected to avoid any losses. Finally, we analyzed the failure modes of the device in order to identify experimental conditions for robust performances. We identified three situations that lead to poor delivery of droplets (Supp. Movie 6). The first case occurred when droplets injected into the device were improperly spaced. The presence of many droplets in the bypass channel results in the escape of the trapped droplet. This problem could be easily alleviated by lowering the emulsion to spacing oil pressure ratio to increase droplet spacing, and adjust droplet velocity into the optimal trapping range by adjusting the combined emulsion and spacing oil pressures. The second case was caused by small droplets that got trapped and prevented the capture of a droplet with the proper size. It highlights the need for a mono-disperse emulsion and supports our strategy of using two different oil formulations for generation-collection-storage of droplets and for the emulsion re-injection which permits to maintain a very high mono-dispersity of the emulsion. The last issue occurred when air, injected by the delivery control after a trapping-delivery valve was opened, displaced a droplet out of its trapping chamber. This problem stresses the importance of timing during the delivery sequence and it could be corrected by introducing proper delays (usually a few seconds) between different actuations.

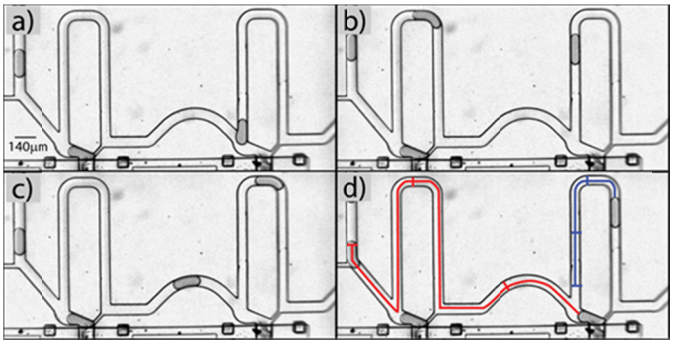

Fig. 6 Auto-correction of multiplex droplet trapping. The delivery system has an intrinsic correction mechanism. a) A droplet skips a trap. b) This droplet flows into the bypass channel where it is greatly slowed down. c) The following droplet flows at higher velocity and catches up. d) When the following droplet reaches the trap, the first droplet still blocks the bypass channel and ensures that the following droplet enters the trap. The paths followed by each droplet (depicted in blue and red) clearly show the differential in velocity. The sequential segments on each trace show the position of droplets in panel a,b and c.

The cycling time of the 8-plex delivery device described is 80 seconds when controlled in a semi-automated fashion where the three sequences of events (loading, clearing, ejecting) that make the complete cycle are pre-programmed but switching between the sequences is triggered by the operator. The device operation is robust enough that the whole cycle could be automated by assigning proper timing to each of the three sequences and automatically cycling through them. Complete discussion of the cycling time needs to take into account the whole delivery system including the time taken by droplets to reach their final vessel and the time it would take a robotic arm to move from one row of a microplate to another. Clearly, such optimizations are beyond the scope of this paper whose aim is to report the principles that can be used to assemble a robust multiplex delivery system of droplets that will allow the interfacing of droplet microfluidics with macroscale technologies such as microplates.

Conclusion

We demonstrated and detailed the development of a device that permits the pooling and dispensing of a precise number of microfluidic droplets. In particular, we identified the key parameters that allow decreasing the cycling time of droplet delivery. This entailed optimizing the design of the trapping chamber and adapting the oil formulation to improve the efficiency of the droplet trapping, uncoupling the loading-clearing and delivery phases, using air for rapid droplet delivery, and multiplexing droplet delivery. The device is robust, versatile and allows pooling and dispensing into multiple dispensing channels. These properties and the fact that operations can be automated for continuous operations are very appealing for interfacing droplet microfluidics with lower throughput technologies such as microtiter plate technology. We anticipate that our design will allow seamless integration of droplet microfluidics into workflows based on macroscale technologies. The work presented here represents a significant step towards the manipulation of an intermediate number of droplets that is critical for low-throughput and sample preparation applications where throughput needs to be traded for higher control of droplet manipulation. In particular, we aim at using this platform to facilitate the sample preparation of single-cells for genomic applications. The miniaturized platform presented here would also provide the basis for the development of analytical devices for multiplexed point-of-care diagnostics.

Acknowledgements

Research carried out in part at the Center for Functional Nanomaterials, Brookhaven National Laboratory, which is supported by the U.S. Department of Energy, Office of Basic Energy Sciences, under Contract No. DE-AC02-98CH10886." This research was supported by funds from The Center for Biotechnology, an Empire State Development, Division of Science, Technology and Innovation (NYSTAR), Center for Advanced Technology, a grant from NIH-NHGRI (R21 HG006206), a grant from NIH-NCI (R01 CA181595), and a grant from NSF (DMR-Award 1106044). EB received some support from the Simons Foundation. We would like to thank Professor Thomas Cubaud (Stony Brook University) for useful discussions.

Notes and references

[a] Biomedical Engineering Department, Stony Brook University, Stony Brook, NY 11794-5281.
*: Corresponding author. eric.brouzes@stonybrook.edu

Electronic Supplementary Information (ESI) available: Supplemental calculations, figures and movies. See DOI: 10.1039/b000000x/

1. S. L. Anna, N. Bontoux and H. A. Stone, *Applied Physics Letters*, 2003, 82, 364-366.
2. T. Thorsen, R. W. Roberts, F. H. Arnold and S. R. Quake, *Phys Rev Lett*, 2001, 86, 4163-4166.
3. A. N. Banerjee, S. Qian and S. W. Joo, *Journal of Colloid and Interface Science*, 2011, 362, 567-574.
4. B. Hadwen, G. R. Broder, D. Morganti, A. Jacobs, C. Brown, J. R. Hector, Y. Kubota and H. Morgan, *Lab on a Chip*, 2012, 12, 3305-3313.
5. L. Malic, D. Brassard, T. Veres and M. Tabrizian, *Lab on a Chip*, 2010, 10, 418-431.
6. Y. Marcy, C. Ouverney, E. M. Bik, T. Losekann, N. Ivanova, H. G. Martin, E. Szeto, D. Platt, P. Hugenholtz, D. A. Relman and S. R. Quake, *Proc Natl Acad Sci U S A*, 2007, 104, 11889-11894.
7. J. Melin and S. R. Quake, *Annu Rev Biophys Biomol Struct*, 2007, 36, 213-231.
8. M. A. Unger, H. P. Chou, T. Thorsen, A. Scherer and S. R. Quake, *Science*, 2000, 288, 113-116.
9. A. Huebner, S. Sharma, M. Srisa-Art, F. Hollfelder, J. B. Edel and A. J. Demello, *Lab Chip*, 2008, 8, 1244-1254.
10. A. B. Theberge, F. Courtois, Y. Schaerli, M. Fischlechner, C. Abell, F. Hollfelder and W. T. S. Huck, *Angewandte Chemie International Edition*, 2010, 49, 5846-5868.
11. J. J. Agresti, E. Antipov, A. R. Abate, K. Ahn, A. C. Rowat, J. C. Baret, M. Marquez, A. M. Klibanov, A. D. Griffiths and D. A. Weitz, *Proc Natl Acad Sci U S A*, 2010, 107, 4004-4009.
12. S. L. Sjostrom, Y. Bai, M. Huang, Z. Liu, J. Nielsen, H. N. Joensson and H. Andersson Svahn, *Lab Chip*, 2013, DOI: 10.1039/c3lc51202a.
13. B. El Debs, R. Utharala, I. V. Balyasnikova, A. D. Griffiths and C. A. Merten, *Proc Natl Acad Sci U S A*, 2012, 109, 11570-11575.
14. E. Brouzes, M. Medkova, N. Savenelli, D. Marran, M. Twardowski, J. B. Hutchison, J. M. Rothberg, D. R. Link, N. Perrimon and M. L. Samuels, *Proc Natl Acad Sci U S A*, 2009, 106, 14195-14200.
15. J. Clausell-Tormos, D. Lieber, J. C. Baret, A. El-Harrak, O. J. Miller, L. Frenz, J. Blouwolff, K. J. Humphry, S. Koster, H. Duan, C. Holtze, D. A. Weitz, A. D. Griffiths and C. A. Merten, *Chem Biol*, 2008, 15, 427-437.
16. S. Koster, F. E. Angile, H. Duan, J. J. Agresti, A. Wintner, C. Schmitz, A. C. Rowat, C. A. Merten, D. Pisignano, A. D. Griffiths and D. A. Weitz, *Lab Chip*, 2008, 8, 1110-1115.
17. H. N. Joensson, M. L. Samuels, E. R. Brouzes, M. Medkova, M. Uhlen, D. R. Link and H. Andersson-Svahn, *Angewandte Chemie*, 2009, 48, 2518-2521.
18. T. Geng, R. Novak and R. A. Mathies, *Analytical chemistry*, 2014, 86, 703-712.
19. Y. Zeng, R. Novak, J. Shuga, M. T. Smith and R. A. Mathies, *Analytical chemistry*, 2010, 82, 3183-3190.
20. N. Navin, J. Kendall, J. Troge, P. Andrews, L. Rodgers, J. McIndoo, K. Cook, A. Stepansky, D. Levy, D. Esposito, L. Muthuswamy, A. Krasnitz, W. R. McCombie, J. Hicks and M. Wigler, *Nature*, 2011, 472, 90-94.
21. Y. Marcy, T. Ishoey, R. S. Lasken, T. B. Stockwell, B. P. Walenz, A. L. Halpern, K. Y. Beeson, S. M. Goldberg and S. R. Quake, *PLoS Genet*, 2007, 3, 1702-1708.
22. H. Boukellal, S. Selimovic, Y. Jia, G. Cristobal and S. Fraden, *Lab on a Chip*, 2009, 9, 331-338.
23. A. Huebner, D. Bratton, G. Whyte, M. Yang, A. J. deMello, C. Abell and F. Hollfelder, *Lab on a Chip*, 2009, 9, 692-698.
24. A. R. Abate, J. J. Agresti and D. A. Weitz, *Applied Physics Letters*, 2010, 96.
25. K. Leung, H. Zahn, T. Leaver, K. M. Konwar, N. W. Hanson, A. P. Page, C. C. Lo, P. S. Chain, S. J. Hallam and C. L. Hansen, *Proc Natl Acad Sci U S A*, 2012, 109, 7665-7670.
26. M. G. Simon, R. Lin, J. S. Fisher and A. P. Lee, *Biomicrofluidics*, 2012, 6, 14110-1411013.
27. E. Brouzes, *Methods Mol Biol*, 2012, 853, 105-139.
28. P. M. Fordyce, C. A. Diaz-Botia, J. L. DeRisi and R. Gomez-Sjoberg, *Lab Chip*, 2012, 12, 4287-4295.
29. J. Clausell-Tormos, A. D. Griffiths and C. A. Merten, *Lab on a Chip*, 2010, 10, 1302-1307.
30. L. Frenz, K. Blank, E. Brouzes and A. D. Griffiths, *Lab on a Chip*, 2009, 9, 1344-1348.
31. C. Holtze, A. C. Rowat, J. J. Agresti, J. B. Hutchison, F. E. Angile, C. H. Schmitz, S. Koster, H. Duan, K. J. Humphry, R. A. Scanga, J. S. Johnson, D. Pisignano and D. A. Weitz, *Lab Chip*, 2008, 8, 1632-1639.
32. P. Abbyad, R. Dangla, A. Alexandrou and C. N. Baroud, *Lab Chip*, 2011, 11, 813-821.
33. R. Dangla, S. Lee and C. N. Baroud, *Physical Review Letters*, 2011, 107, 124501.